Behavioral/Cognitive

Dissociation between Attention-Dependent and Spatially Specific Illusory Shape Responses within the Topographic Areas of the Posterior Parietal Cortex

Ana Arsenovic,[1,2] Anja Ischebeck,[1,2] and Natalia Zaretskaya[1,2]

[1]Department of Cognitive Psychology and Neuroscience, Institute of Psychology, University of Graz, 8010 Graz, Austria, and [2]BioTechMed-Graz, 8010 Graz, Austria

The human visual system consists of multiple topographic maps that extend from the early visual cortex (EVC) along the dorsal and ventral processing streams. Responses to illusory shapes within these maps have been demonstrated in the ventral stream areas, in particular the lateral occipital complex (LOC). Recently, the intraparietal sulcus (IPS) of the dorsal stream has been linked to the processing of illusory shapes defined by motion. It remains unclear whether the topographically organized parietal areas also respond to stationary illusory shapes, which would suggest their generic role in representing illusory content. In the current study we measured brain responses using fMRI while 30 human participants (12 male) observed flickering inducers around the fixation task. The inducers either formed an illusory diamond in the center, a triangle in the left or right hemifield, or were inverted such that no illusory figure was formed. We compared responses of parietal regions IPS0-IPS5 and SPL1 to each illusory figure with the nonillusory condition. To determine the role of attentional modulation on illusory shape responses we manipulated the difficulty of the fixation task. Our results show that all IPS areas responded to illusory shapes. The more posterior areas IPS0–IPS3 additionally displayed a preference toward contralateral shapes, while the more anterior areas IPS4 and IPS5 showed response attenuation with increased task difficulty. We suggest that the IPS can represent illusory content generated not only by moving, but also by stationary stimuli, and that there is a functional dissociation between attention-dependent anterior and spatially specific posterior topographic maps.

Key words: **fMRI; illusory shapes; intraparietal sulcus; Kanizsa figure; posterior parietal cortex**

Significance Statement

The traditional view of the ventral visual pathway being solely responsible for representation of objects has recently been challenged by demonstrating illusory shape representation within the dorsal visual pathway with moving bistable stimuli. Our results provide evidence for the dorsal stream contribution to representing not only moving, but also stationary illusory shapes. Our results also show a functional subdivision along the topographic maps, with spatially specific shape responses in the more posterior, and attention-dependent responses in the more anterior areas. These findings have implications for our understanding of the relationship between attention and grouping in healthy individuals and neuropsychological patients. Furthermore, IPS areas should be considered in theoretical accounts and models of how subjective content is generated in the brain.

Introduction

One of the fundamental principles of brain organization is topography. Each sensory modality contains multiple topographic maps, which are considered to be central to information processing within the respective modality (Kaas, 1997; Silver and Kastner, 2009). Functional magnetic resonance imaging of the visual system revealed the visual topographic organization far beyond the early visual cortex (EVC). Currently, >30 topographic maps have been identified across the visual processing hierarchy, extending from subcortical visually responsive areas (Schneider et al., 2004; DeSimone et al., 2015) and the EVC (Sereno et al., 1995; Engel et al., 1997), up to the parahippocampal areas along

Received Apr. 11, 2022; revised July 31, 2022; accepted Aug. 22, 2022.

Author contributions: A.A. and N.Z. designed research; A.A. and N.Z. performed research; A.A. analyzed data; A.A. wrote the first draft of the paper; A.A., A.I., and N.Z. edited the paper; A.A., A.I., and N.Z. wrote the paper.

This work was supported by a BioTechMed-Graz Young Researcher Group grant. We thank Thomas Zussner for his help during MR data acquisition.

The authors declare no competing financial interests.

Correspondence should be addressed to Ana Arsenovic at ana.arsenovic@uni-graz.at or Natalia Zaretskaya at natalia.zaretskaya@uni-graz.at.

https://doi.org/10.1523/JNEUROSCI.0723-22.2022

the ventral stream and the frontal eye fields along the dorsal stream (Wang et al., 2015). The exact functional role of these maps remains a topic of debate (Wandell et al., 2007).

Previous studies have shown that topographic maps in the EVC can represent not only simple sensory features (e.g., orientation, color, motion direction), but also more complex illusory content, i.e., aspects of perception than cannot be explained by the bottom-up input. For example, the EVC shows responses not only to physical, but also to illusory contours (von der Heydt et al., 1984; Larsson et al., 1999; Zhou et al., 2000; Lee and Nguyen, 2001; Maertens et al., 2008). Furthermore, it shows response enhancement within the topographic representation of the illusory surface and suppression at the location of the inducers and the background (Kok and de Lange, 2014; Kok et al., 2016; Grassi et al., 2017). This complex response pattern in the EVC is thought to be a result of feedback modulation from higher-level areas, which also respond to illusory contours (Mendola et al., 1999; Murray et al., 2002; Anken et al., 2018).

According to the two-streams hypothesis, the perception of shapes, including illusory shapes, is a function of the ventral stream (Haxby et al., 1991; Goodale and Milner, 1992). Indeed, multiple studies have demonstrated the involvement of the lateral occipital complex (LOC) in the perception of not only real, but also illusory shapes (Stanley and Rubin, 2003; Murray et al., 2004; de-Wit et al., 2009; Chen et al., 2020), making it a candidate area for providing the feedback signal to early visual areas (Fang et al., 2008; Wokke et al., 2013). However, the strict dichotomy between the ventral and the dorsal stream in the context of object perception is being continuously challenged (Freud et al., 2016). Recently, several studies reported activity in the posterior parietal cortex (PPC) and, more specifically, in the intraparietal sulcus (IPS) of the dorsal stream during perception of illusory shapes (Zaretskaya et al., 2013; Zaretskaya and Bartels, 2015; Grassi et al., 2018). These studies used bistable stimuli which can be interpreted either as an illusory global shape or as local nonillusory elements based on the same sensory input. Crucially, the illusory shapes investigated in these studies were defined by motion cues, which are expected to be processed along the dorsal stream. The PPC is known to contain multiple attention-defined topographic maps (Sereno et al., 2001; Schluppeck et al., 2005; Silver et al., 2005; Swisher et al., 2007; Konen and Kastner, 2008), which likely overlapped with previously reported activations. It is therefore unclear whether the topographic areas of the PPC also respond to stationary illusory shapes and whether these responses depend on attention, which illusory shapes are known to capture (Senkowski et al., 2005; Kimchi et al., 2016).

In this study, we were interested in whether parietal topographic areas respond to stationary illusory Kanizsa shapes (Kanizsa, 1976) and how these responses are modulated by top-down attention. We conducted an fMRI study in which we measured brain responses of human participants while they viewed Kanizsa figures and performed a central fixation task. By independently manipulating the figure location and task difficulty, we were able to dissociate the shape-related from the attention-dependent parietal activity.

Materials and Methods

Participants

Thirty healthy volunteers (12 male), aged 19–31 years (M = 23.53 ± 2.92 SD), participated in the experiment. We performed an a priori power analysis using GPower 3.1.9.7 (Faul et al., 2007) to determine the sample size, based on a previous fMRI study involving illusory content within the PPC (Grassi et al., 2018). Based on the smallest effect size reported within the PPC (Cohen's $d = 0.59$), with an α level of 0.05 and 80% power, at least 25 participants would be required for a two-tailed paired t test. Thus, our sample was sufficient to test the hypotheses of this study. All but one of the participants were right-handed. All participants had normal or corrected-to-normal vision and did not take any psychotropic medications at the time. Before the experiment, the participants were prescreened for MRI contraindications and had signed a written informed consent form. The study was conducted according to the Declaration of Helsinki and the study's procedure and protocols were approved by the ethics committee of the University of Graz. The current study represents a part of a bigger project, which was preregistered before data collection (https://aspredicted.org/ke4b9.pdf).

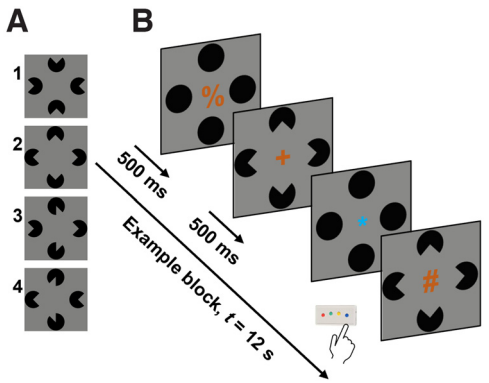

Figure 1. Stimulus types and experimental paradigm. ***A***, Stimuli arranged in four possible inducer configurations: (1) no illusion, (2) diamond, (3) right triangle, and (4) left triangle. ***B***, Sequence of events within one example experimental block. The example block represents diamond inducer configuration continuously flickering around the easy detection task. Participants fixated centrally positioned symbols and responded to changes in symbol color; t, block duration. The proportions in this figure are altered for illustration purposes.

Stimuli and task

Visual stimuli were generated using MATLAB R2019b (MathWorks, 2019) and Psychophysics Toolbox 3 (Brainard, 1997; Pelli, 1997; Kleiner et al., 2007) on a Linux computer (Ubuntu 18.04 LTS). The stimuli were presented in the MR scanner room on a 32″ γ-corrected monitor (resolution: 1920 × 1080 pixels, refresh rate: 60 Hz, maximum surface luminance: 405 cd/m^2, Nordic NeuroLab), which was viewed via a mirror mounted above the head coil. The total distance from the display to the eyes of the participants was 143.5 cm. Before entering the scanner room, we ensured sufficient visual acuity of each participant with the Snellen chart. We gave the participants a thorough instruction regarding the detection task (see below) and advised them not to move their head during the entire MRI acquisition.

In each experimental block, we presented one of the four possible stimulus configurations ("no illusion," "diamond," "left triangle," and "right triangle"; Fig. 1*A*) on the screen for a total of 12 s. Each stimulus consisted of four black (RGB (Red, Green, Blue): 0, 0, 0) pac-man inducer combinations, which were presented against a gray background (RGB: 128, 128, 128). Each inducer consisted of a circle shape with a cut out wedge and subtended 4.08° of visual angle. The inducers were arranged in a diamond shape around the central fixation circle at an eccentricity of 5.77° of visual angle in four possible configurations that yielded four experimental conditions. In the "no illusion" configuration, all inducers were oriented with the 90° cut out wedge facing outwards, thus not creating an illusory shape in the center. In the "diamond" configuration, the inducers were aligned to form a centrally positioned illusory diamond shape. In the "left triangle" configuration, top and bottom inducers had a 45° cut out wedge and were rotated such that an illusory triangle formed within the left visual hemifield. The "right triangle" configuration was a vertically flipped version of the left triangle configuration resulting in an illusory triangle within the right visual hemifield. To account for adaptation in the visual cortex, the stimuli were continuously

flickering between pac-man inducers and full circles every 500 ms throughout each experimental block.

To ensure central gaze fixation and equal distribution of attention across the stimulus conditions, participants performed a central detection task. A stream of orange (RGB: 153, 80, 0) and blue (RGB: 0, 107, 209) symbols subtending 0.6° of visual angle was presented at the center of the display. A pseudo-randomly chosen symbol was presented one at a time from a fixed set of 26 possible symbols (!"$%&/()=?{[]}\+*~#-:;><@^). Each symbol was presented for 12 frames (~200 ms) on the screen. The participants were instructed to always attend to the centrally positioned stream of symbols. Participants had to perform one of the two tasks, which remained the same throughout one run. In the first task ("easy"), participants were instructed to press a button on the response box in their hand each time the symbol color changed to blue (5% of all symbols), regardless of the symbol identity. In the second task ("hard"), the participants were instructed to press the button each time the plus symbol ("+") appeared on the screen (5% of all symbols), regardless of its color. On average, target symbols appeared around three times per block in either task. The symbol stream appearance and target frequency were thus identical in the two task conditions, and only the task demands varied. The sequence of events within one block can be seen in Figure 1*B*.

Each of the four stimulus configurations (block) was presented six times per run. The sequence of experimental blocks was determined for each run by generating a first-order counterbalanced sequence of conditions (Brooks, 2012). Baseline blocks (12 s each) were added after every fourth experimental block, with a total of six baseline blocks per run. During the baseline blocks, a central fixation point was presented in place of the symbol stream and nonflickering black circles were presented in place of pac-man inducers. In total, there were 30 blocks in each run. The total duration of one run was 360 s (excluding the four initial dummy scans, which were subsequently discarded). Between each run there was a short (1–2 min) break, during which the participants could rest their eyes. In total, one scanning session included eight experimental runs (four runs per task condition). The order of runs with easy and hard detection tasks was pseudorandomized and counterbalanced between the participants. Additionally, after the main experiment we collected an anatomical MRI scan for each participant. The total duration of the whole session was around 60 min.

After the MRI acquisition, participants received a questionnaire with six questions for assessment of their subjective visual experience during the experiment. The participants rated the perceived difficulty of the tasks and the subjective strength of illusory figures on a Likert scale ranging from 1 to 6. The questionnaire included the following questions: "Please rate your subjective perception of the difficulty of the," Q1: "symbol task"; Q2: "color task" (1, not difficult at all; 6, very difficult). "During the experiment, how strongly did you perceive the following illusory figures?" Q3: "illusory diamond during the symbol task"; Q4: "illusory diamond during the color task"; Q5: "illusory triangles during the color task"; Q6: "illusory triangles during the symbol task" (1, not at all; 6, very strongly).

MRI data acquisition

Neuroimaging data were acquired using a 3T Siemens MAGNETOM Vida scanner (Siemens Healthineers) with a 64-channel head coil. Functional MRI scans were acquired using the simultaneous multislice (SMS) accelerated echo-planar imaging (EPI) sequence using T2*-weighted blood oxygenation level-dependent (BOLD) contrast (58 axial slices, TR = 2000 ms, TE = 30 ms, FOV = 220 mm, flip angle = 82°, voxel size = 2.0 × 2.0 × 2.0 mm, SMS factor 2). To compensate for distortion correction during preprocessing, we also acquired one EPI image with opposite phase encoding direction (P ≫ A). Additionally, a high-resolution anatomical scan was acquired using the T1-weighted (T1w) MPRAGE sequence (TR = 2530 ms, TE = 3.88 ms, TI = 1200 ms, voxel size: 1.0 × 1.0 × 1.0 mm, GRAPPA factor 2).

MRI data preprocessing

Before any data preprocessing, we removed facial identifiers from all participants with pydeface 2.0.0 (Gulban et al., 2019). Afterwards, we visually inspected the quality of MRI images with MRIQC 0.16.1 (Esteban et al., 2017). Anatomical and functional MRI data were preprocessed using fMRIPrep 20.2.3 (Esteban et al., 2019), which is based on Nipype 1.6.1 (Gorgolewski et al., 2011). The main preprocessing steps are summarized below.

Anatomical data preprocessing

The T1w image was corrected for intensity nonuniformity with ANTs *N4BiasFieldCorrection* function and used as T1w-reference, which was then skull-stripped. CSF, white-matter (WM), and gray-matter (GM) brain tissue segmentation was performed on the brain-extracted T1w using *fast* function from FSL 5.0.9 (Woolrich et al., 2009). Brain surfaces were reconstructed using FreeSurfer *recon-all* function (Dale et al., 1999).

Functional data preprocessing

First, a reference volume and its skull-stripped version were generated using a custom methodology of fMRIPrep. For each BOLD run the following preprocessing transformations were performed: A B0-nonuniformity map was estimated based on the EPI with opposite phase-encoding direction using *3dQwarp* from AFNI 20160207 (Cox, 1996). Based on the estimated susceptibility distortion, a corrected EPI reference was calculated for more accurate co-registration with the anatomic reference. The BOLD reference image was co-registered to the T1w reference image using FreeSurfer's *bbregister* (Greve and Fischl, 2009). Head-motion parameters with respect to the BOLD reference image were estimated before any spatiotemporal filtering using *mcflirt* (FSL 5.0.9). Slice-time correction was performed using *3dTshift* from AFNI 20160207. These transforms were concatenated and applied in one interpolation step. The BOLD-time series were resampled to the fsaverage surface using *mri_vol2surf* (FreeSurfer). For the region of interest (ROI) general linear model (GLM) analyses (see below), we used unsmoothed preprocessed BOLD runs. For the whole-brain GLM analyses, each preprocessed BOLD run was smoothed along the cortical surface with a 2D Gaussian kernel of 5-mm full-width at half-maximum (FWHM) using *mri_surf2surf* (FreeSurfer).

Data analysis

First-level GLM analysis

All first-level GLM analyses were performed using FsFast (FreeSurfer Functional Analysis Stream). For each participant, we performed a standard GLM analysis, with each experimental condition modeled as a unique regressor convolved with a canonical hemodynamic response function (HRF). In contrast to early visual areas, areas of the superior parietal cortex are known to show a transient BOLD response pattern (Steinman et al., 1997; Yantis et al., 2002; Zaretskaya et al., 2013), which we confirmed for our paradigm with an additional finite impulse response GLM analysis. Thus, we modeled experimental conditions in the GLM as 0.1 s events at block onsets rather than full 12-s block durations. There were eight unique condition regressors in total, with the first four modeling stimulus configurations under the hard task (no illusion, diamond, left triangle, right triangle) and the next four under the easy task (no illusion, diamond, left triangle, right triangle). Additionally, run-specific effects as well as slow signal drifts were added as nuisance regressors. Illusory shape activity was quantified by calculating six contrast estimates (CES). The latter were defined as the difference of β estimates between each illusory shape condition (diamond, left triangle and right triangle) and the "no illusion" condition, separately for each task type. The resulting contrasts thus represent illusory shape-related activity after accounting for the overall effects of task, which should cancel in the task-specific subtraction. The GLM was fit to the unsmoothed data for the ROI analysis. All statistical analyses and plotting were performed in RStudio 4.1.2 (RStudio Team, 2021). Where appropriate, error bars were plotted with confidence intervals (CIs) adjusted for within-subject design using the Cousineau-Morey method (Morey, 2008).

Definition of ROIs and ROI analysis

Seven topographic areas of the PPC (IPS0, IPS1, IPS2, IPS3, IPS4, IPS5, and SPL1) were defined using the maximum probability maps (MPM)

of the surface-based probabilistic atlas by Wang et al. (2015), resampled to FreeSurfer fsaverage standard space (Benson and Winawer, 2018). Since our study is hypothesis-driven, an a priori definition of the parietal areas via probabilistic MPMs is a recommended method for inferring the individual's anatomic locations within the brain (Eickhoff et al., 2006). Furthermore, the predefined areas in a standard surface space allow for unbiased and direct comparison with data from other studies (Wang et al., 2015). Figure 2*A* illustrates the location of ROIs on an inflated cortical surface. The number of vertices for each parietal ROI were: IPS0 = 1055, IPS1 = 900, IPS2 = 899, IPS3 = 604, IPS4 = 148, IPS5 = 53, and SPL1 = 232 vertices in the left hemisphere and IPS0 = 835, IPS1 = 675, IPS2 = 624, IPS3 = 805, IPS4 = 160, IPS5 = 18, and SPL1 = 295 vertices in the right hemisphere. We extracted mean values over vertices within each ROI for each contrast estimate map of each participant. The per-ROI means were then used to conduct statistical analysis. Since we do not expect a lateralization of the illusory diamond response, we averaged mean shape response over both hemispheres. For the illusory triangle response, we averaged the two contralateral triangle values (i.e., the left hemisphere value for the contrast "right triangle > no illusion" and the right hemisphere value for the contrast "left triangle > no illusion") and the two ipsilateral values (i.e., the left hemisphere value for the contrast "left triangle > no illusion" and the right hemisphere value for the contrast "right triangle > no illusion").

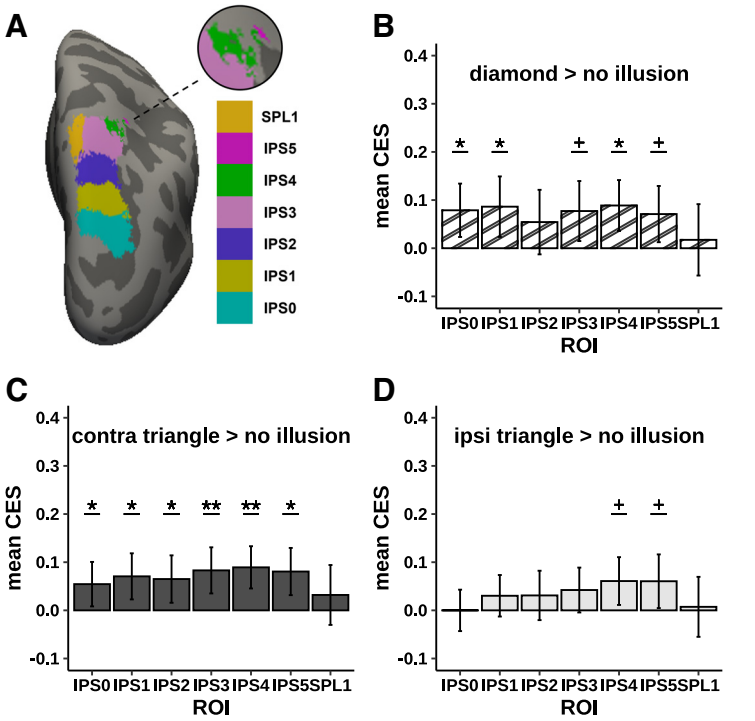

Figure 2. Illusory shape responses in parietal topographic maps (easy task). ***A***, Location of the parietal areas from the probabilistic surface-based atlas (Wang et al., 2015), overlayed onto the right hemisphere of the inflated fsaverage cortical surface. Inset shows enlarged anterior areas IPS4 and IPS5. ***B–D***, Illusory shape-related response during the easy task within the PPC (***B***, diamond, both hemispheres; ***C***, triangle, contralateral hemisphere; ***D***, triangle, ipsilateral hemisphere). Error bars represent 95% CIs; $^{+}p < 0.05$, uncorrected; $^{*}p < 0.05$, $^{**}p < 0.01$, Holm–Bonferroni corrected (7 tests).

The following statistical tests were conducted to investigate the illusory shape response in the parietal ROIs. First, we tested the presence of illusory shape responses in each parietal ROI by testing for non-zero contrast differences ("diamond > no illusion," "contralateral triangle > no illusion," and "ipsilateral triangle > no illusion") during the easy task with a two-tailed one sample *t* test. Second, we tested the spatial specificity of the illusory shape response within each ROI by comparing contralateral and ipsilateral responses during the easy task with a two-tailed paired samples *t* test. Third, we tested whether higher task demands affected illusory diamond responses by directly comparing diamond responses for the two task difficulties with a two-tailed paired samples *t* test within each ROI. Finally, we tested whether higher task demands affected illusory triangle response by performing a 2 × 2 repeated-measures ANOVA within each ROI, with laterality (contralateral and ipsilateral) and task (easy and hard) as factors. All *t* tests and ANOVA factors were corrected for multiple comparisons using Holm–Bonferroni method (Holm, 1979) and the corrected statistics are labeled in the figures. All raw *p*-value counterparts of the corrected statistics are also included either directly in the text or in a table.

Additional whole-brain group analysis

To confirm previous findings on illusory shape response in the ventral and early visual areas we performed an additional whole-brain group analysis. The analysis was performed using FreeSurfer *mri_glmfit* command with -wls flag (weighted-least-squares), testing for non-zero differences. To test for the presence of the illusory shape response, we compared all illusory shape conditions with the no illusion condition during the easy task (**C** = [0 0 0 0 −1 0.333 0.333 0.333]). To test for spatial specificity of shape responses, we compared the left triangle with the right triangle condition during the easy task (**C** = [0 0 0 0 0 0 1 −1]). Finally, to test the impact of task on the illusory shape responses, we compared illusory shape response in easy and in hard task (**C** = [−0.5 0.167 0.167 0.167 0.5 −0.167 −0.167 −0.167]). Correction for multiple comparisons was performed using precomputed z-based Monte Carlo simulation with a cluster-wise threshold at $p < 0.05$ (Hagler et al., 2006) and a cluster-forming threshold at $p < 0.001$ to minimize false positive rates (see Greve and Fischl, 2018). Finally, we adjusted *p*-values with a Bonferroni correction for two spaces (left and right hemisphere). The surviving clusters were classified according to the Desikan–Killiany cortical parcellation (Desikan et al., 2006). Additionally, we calculated the overlap between the clusters and areas of the visual probabilistic atlas (Wang et al., 2015).

Behavioral data analysis

In our behavioral data analysis, we ensured that our manipulation of the task difficulty was successful. The difficulty of both detection tasks was verified with the average hit rate and the participants' subjective rating of the task difficulty. The hit rate in each run was calculated as a total number of correctly detected target instances (target color or target symbol, depending on the task), divided by the total number of target instances and multiplied by 100. Values from the runs with the same task type were averaged. We compared the average hit rates between the easy and the hard task and the subjective ratings of the task difficulty by performing a two-tailed paired samples Wilcoxon signed rank test with continuity correction. To determine whether differences in illusory shape response between tasks observed in fMRI can be explained by differences in subjective experience of the illusory shapes, we also compared participants' ratings of their subjective illusion perception between tasks with two Wilcoxon signed rank tests, one for the diamond and one for the triangle condition.

Our central task was designed to manipulate subjects' attentional demand and test its impact on the processing of illusory shapes. However, the processing of the central targets can be impaired by the presence of the task-irrelevant salient illusory figures in the periphery, yielding an opposite effect (Chen et al., 2019). To ensure that our task manipulation fulfilled its purpose and was equally efficient across different inducer configuration, we additionally analyzed behavioral performance separately for each stimulus configuration and each task. We performed a nonparametric 2 × 4 repeated-measures aligned ranks transformation (ART) ANOVA (Wobbrock et al., 2011) using the ARTool R package (Kay et al., 2021), with the factors of task (easy, hard) and stimulus configuration (no illusion, diamond, left triangle, right triangle).

Additional control analyses

The above behavioral data analysis confirmed the differences in hit rates between the tasks, which means that participants pressed more often during the easy compared with the hard task (because of higher hit rates). To account for the potential role of motor response in explaining our fMRI results, we performed two additional analyses. First, we performed three nonparametric 2×4 repeated-measures ART ANOVAs with the factors of task (easy, hard) and stimulus configuration (no illusion, diamond, left triangle, right triangle) for the average frequency of hits, frequency of misses and frequency of false presses per block. Second, we performed a modified GLM analysis with three additional nuisance regressors containing (1) target hits (modeled as events at button press onset), (2) false presses (modeled as events at button press onset), and (3) missed targets (modeled as events at target onset). Each of these additional regressors was modeled with a duration of 0.1 s. This modified GLM was used to repeat the ROI analysis as described in the main analysis section, but with motor response accounted for. We then compared the overall pattern of results found with this modified GLM with our original ROI results.

Our final control analysis was related to the potential effect of the stimulus flicker itself. The illusory stimuli in our experiment were not defined by motion, but they also were not entirely static because of flicker that we added to the inducers to prevent adaptation of the visual system to the stimulus. Previous research has shown that flickering stationary stimuli can activate area hMT (Tootell et al., 1995), and that areas hMT and MST are more activated by a flickering Kanizsa figure, compared with a flickering no illusion condition (Goebel et al., 1998). To determine whether parietal illusory shape responses in our experiment are related to the flicker, which should engage other dorsal stream areas including the motion-sensitive hMT and MST, we derived the location of these areas using procedures identical to the main analysis (Wang et al., 2015) and tested whether they respond higher to illusory shapes compared with the no illusion condition.

Data and code availability

Video examples of the stimuli, detailed MRI preprocessing steps, ROI and group-level fMRI results, behavioral results, as well as control analyses and relevant scripts are available at the OSF project repository: https://osf.io/n9bjr/. Our institution's data protection policy currently does not allow publicly sharing native space MRI data, but we are able to share the data on direct request from individual researchers.

Results

Illusory shape responses

We first examined whether parietal topographic regions responded to illusory Kanizsa shapes in the easy task, which is comparable to a typical fixation task used in fMRI. We performed a one-sample *t* test for a non-zero illusory diamond response (difference between the illusory diamond and no illusion) in each ROI. Significant illusory shape response was present in areas IPS0, IPS1, IPS3, IPS4 and IPS5. SPL1 and IPS2 did not respond to the illusory diamond (Fig. 2*B*).

The surface of the illusory diamond was occupying the central visual field around the fixation task. It was therefore easy to perceive and potentially captured attention. Thus, we also tested whether illusory shape responses were present in the parietal areas for the triangles which were placed peripherally relative to the central task. All six ROIs of the IPS (IPS0–5) responded to the contralateral illusory triangle during the easy task. SPL1 was not activated by the illusory triangle (Fig. 2*C*). Interestingly, IPS4 and IPS5 also responded to the illusory triangle presented to the ipsilateral hemisphere (Fig. 2*D*). Statistical details about illusory shape responses are presented in Table 1.

Table 1. Illusory shape response (shape > no illusion, easy task)

	Diamond (bilateral)			Triangle (contralateral)			Triangle (ipsilateral)		
ROI	*t*	*p*	*d*	*t*	*p*	*d*	*t*	*p*	*d*
IPS0	2.908	0.007**	0.531	2.413	0.022*	0.44	−0.002	0.998	0
IPS1	2.811	0.009**	0.513	3.018	0.005**	0.551	1.437	0.161	0.262
IPS2	1.657	0.108	0.303	2.701	0.011*	0.493	1.237	0.226	0.226
IPS3	2.534	0.017*	0.463	3.549	0.001**	0.648	1.854	0.074	0.339
IPS4	3.435	0.002**	0.627	4.167	< 0.001***	0.761	2.508	0.018*	0.458
IPS5	2.483	0.019*	0.453	3.363	0.002**	0.614	2.220	0.034*	0.405
SPL1	0.481	0.634	0.088	1.051	0.302	0.192	0.240	0.812	0.044

Two-tailed one sample *t* test (df = 29), mean CES compared against 0 (i.e., no illusory shape response); *d*: Cohen's *d*; $^*p < 0.05$, $^{**}p < 0.01$, $^{***}p < 0.001$, uncorrected.

Spatial specificity of the illusory shape response

Next, we tested whether illusory shape responses were spatially specific by directly comparing responses to the contralateral with responses to the ipsilateral triangle using two-tailed paired samples *t* tests for each ROI. Contralateral responses were stronger in IPS0 ($t_{(29)} = 6.397$, $p < 0.001$, $d = 1.17$), IPS1 ($t_{(29)} = 4.090$, $p < 0.001$, $d = 0.747$), IPS2 ($t_{(29)} = 3.203$, $p = 0.003$, $d = 0.585$), IPS3 ($t_{(29)} = 3.461$, $p = 0.002$, $d = 0.632$), and SPL1 ($t_{(29)} = 2.109$, $p = 0.044$, $d = 0.385$). We found no hemispheric difference in illusory triangle shape response in IPS4 ($t_{(29)} = 1.724$, $p = 0.095$, $d = 0.315$) or IPS5 ($t_{(29)} = 0.964$, $p = 0.343$, $d = 0.176$). The comparison between contralateral and ipsilateral responses is shown in Figure 3.

Attentional modulation of the illusory shape response

Finally, we tested whether the observed illusory shape responses were modulated by task difficulty by comparing responses in the easy task with responses in the hard task. For the illusory triangle, a 2×2 repeated-measures ANOVA with the factors of laterality (ipsilateral, contralateral) and task (easy, hard) revealed that shape-related response in IPS0, IPS1, IPS2, and IPS3 showed a preference for the contralateral stimulus presentation (main effect of laterality IPS0: $F_{(1,29)} = 48.628$, $p < 0.001$, $\eta_p^2 = 0.626$; IPS1: $F_{(1,29)} = 21.705$, $p < 0.001$, $\eta_p^2 = 0.428$; IPS2: $F_{(1,29)} = 10.908$, $p = 0.003$, $\eta_p^2 = 0.273$; IPS3: $F_{(1,29)} = 14.632$, $p < 0.001$, $\eta_p^2 = 0.335$; see Fig. 4*A–D*). Crucially, these lateralized illusory triangle responses were not attenuated by the hard task and there was no interaction between task and laterality. In contrast, IPS4 showed an attenuation of the illusory triangle response during the hard task compared with the easy task (main effect of the task $F_{(1,29)} = 7.726$, $p = 0.009$, $\eta_p^2 = 0.21$; Fig. 4*E*). Crucially, this attenuation occurred regardless of laterality (no main effect of laterality) and there was no interaction between task and laterality. IPS5 revealed a trend in the same direction as IPS4 (Fig. 4*F*), but it did not reach significance (main effect of task $F_{(1,29)} = 3.795$, $p = 0.061$, $\eta_p^2 = 0.116$). SPL1 did not show any significant effects. Figure 4*G* shows the graphical representation of the significant main effects for each IPS area.

To determine whether higher attentional demands reduced the illusory diamond response, we compared the responses across different task difficulties with a two-tailed paired samples *t* test for each ROI. However, we found no effect of task on the illusory diamond response in any of the seven parietal ROIs (IPS0: $t_{(29)} = 0.961$, $p = 0.345$, $d = 0.175$; IPS1: $t_{(29)} = 0.656$, $p = 0.517$, $d = 0.120$; IPS2: $t_{(29)} = 0.544$, $p = 0.590$, $d = 0.099$; IPS3: $t_{(29)} = 1.050$, $p = 0.303$, $d = 0.192$; IPS4: $t_{(29)} = 1.286$, $p = 0.209$, $d = 0.235$; IPS5: $t_{(29)} = 0.237$, $p = 0.814$, $d = 0.043$; SPL1: $t_{(29)} = 0.242$, $p = 0.810$, $d = 0.044$).

Behavioral results

Our behavioral results confirmed that our manipulation of task difficulty was successful. A Wilcoxon signed rank test showed a significant difference in hit rates between the two detection tasks ($Z = 4.772$, $p < 0.001$, $r = 0.873$), with the easy task runs having higher hit rates than the hard task runs (Fig. 5*A*). Corresponding effects were found in another Wilcoxon test for the subjective difficulty ratings as well, with the easy task being perceived as easier compared with the hard task ($Z = -3.818$, $p < 0.001$, $r = 0.716$; Fig. 5*B*). Another two separate Wilcoxon signed rank tests with continuity correction comparing subjective illusion strength revealed no difference in illusion strength between the tasks (diamond: $Z = 0.133$, $p = 0.894$, $r = 0.076$; triangle: $Z = -0.619$, $p = 0.536$, $r = 0.111$). Finally, we tested whether hit rates in each stimulus configuration and task variant differ from each other. A 2×4 ART ANOVA on the hit rate showed that the surrounding stimulus configuration did not change the difference in hit rates between the easy and the hard task. There was a significant main effect of the task $F_{(1,232)} = 139.682$, $p < 0.001$, $\eta_p^2 = 0.376$, but no effect of the stimulus configuration ($p = 0.818$) and no interaction ($p = 0.723$; Fig. 5*C*).

Whole-brain results

To check whether our paradigm produces an expected pattern of brain activity outside of IPS, we additionally performed a whole-brain analysis that paralleled our ROI analysis. We found illusory shape-related responses during the easy task in both hemispheres in the EVC (V1–V3) and in areas hV4, V3b and LO1, confirming findings of multiple previous studies. Furthermore, 18 vertices within the left LO2 area also responded to the illusory shapes. Only one of the clusters that survived correction for multiple comparisons was located in the parietal cortex (cluster size: 205 vertices, peak MNI coordinates: [21.7 −57.9 56.6]). The cluster overlaps with the parietal area IPS3 (129 vertices, 62.9% of the cluster vertex size) and IPS4 (67 vertices, 32.68% of the cluster vertex size). Whole-brain group results with significant clusters for the shape response are shown in Figure 6*A*. For the sake of comparison with previous findings, we also compared the location of this parietal cluster with two parietal clusters related to illusory shape perception reported in Zaretskaya et al. (2013). 205 vertices of the "SPL" cluster from their study (16.69% of the total "SPL" vertex size) overlaps with our parietal cluster, and there is no overlap with the "aIPS" cluster from the same study.

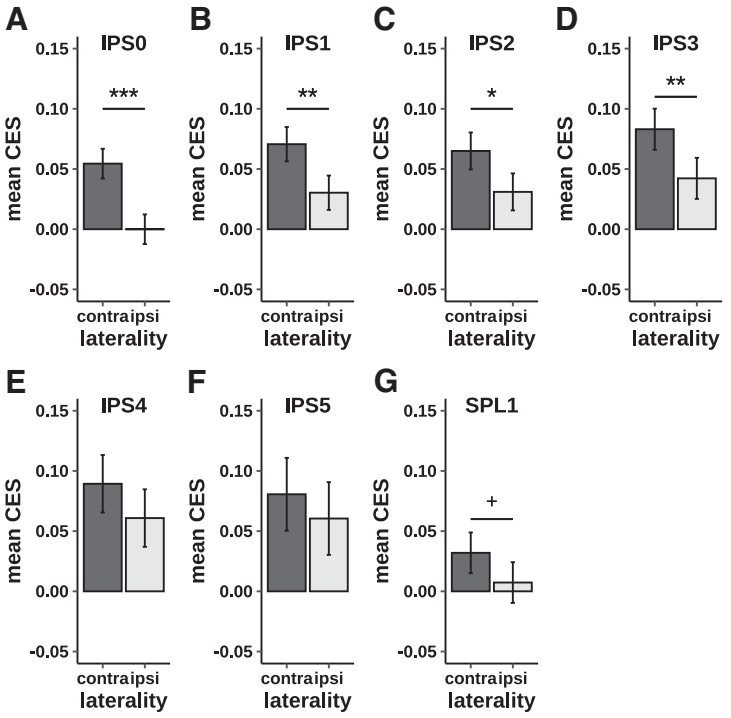

Figure 3. ***A–G***, Spatial specificity of illusory shape responses (easy task). Error bars represent 95% CIs (Morey, 2008); $^{+}p < 0.05$, uncorrected; $^{*}p < 0.05$, $^{**}p < 0.01$, $^{***}p < 0.001$, Holm–Bonferroni corrected (7 tests).

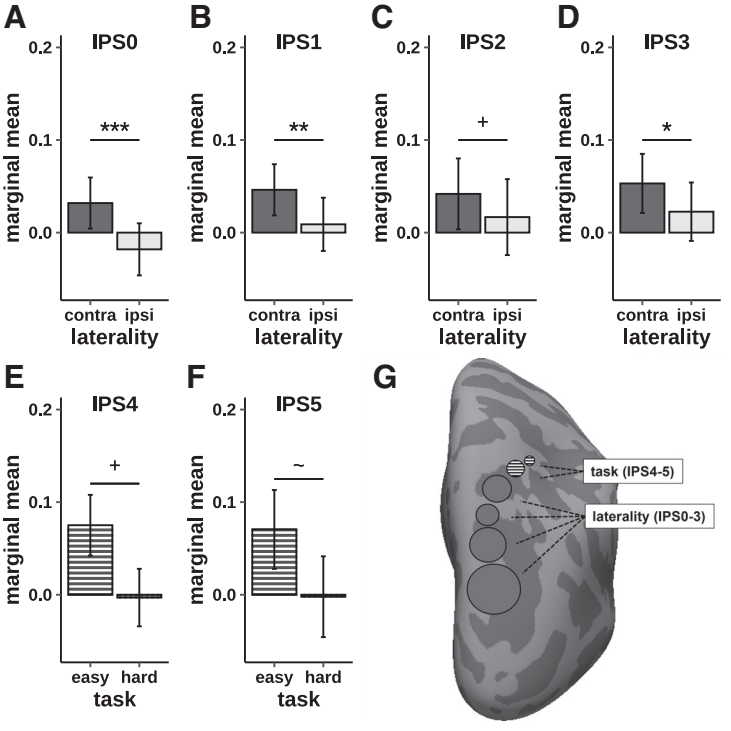

Figure 4. Spatial specificity and task effects in the IPS. ***A–D***, Main effect of laterality in areas IPS0–3. ***E***, ***F***, Main effect of task in area IPS4 and trend of main effect of task in IPS5. Error bars represent 95% CIs (Morey, 2008); $^{\sim}p = 0.061$, $^{+}p < 0.05$, uncorrected; $^{*}p < 0.05$, $^{**}p < 0.01$, $^{***}p < 0.001$, Holm–Bonferroni corrected (21 effects). ***G***, Visualization of the location of the main effects of laterality and task within the PPC on the right inflated cortical surface. The circle size is proportional to the respective effect size.

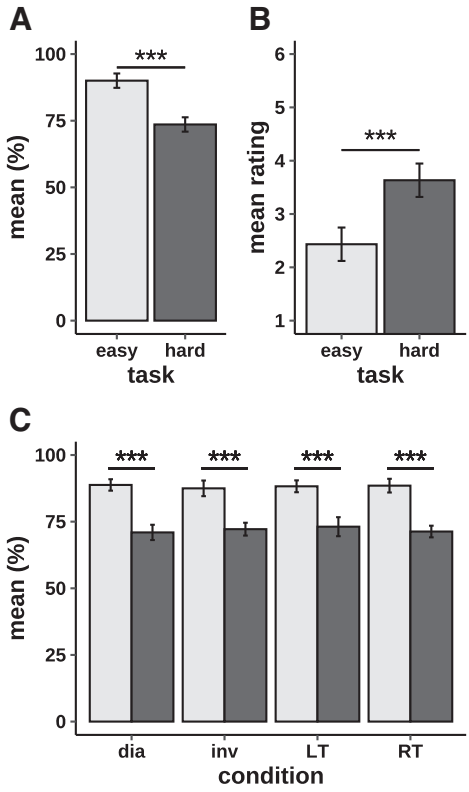

Figure 5. Objective and subjective measurements of task difficulty. ***A***, Total mean hit rate in easy and hard detection tasks. ***B***, Mean ratings of subjective task difficulty, rated on a six-point Likert scale (1, not difficult at all; 6, very difficult). ***C***, Hit rate per stimulus configuration. dia, diamond; inv, no illusion; LT, left triangle; RT, right triangle. Error bars represent 95% CIs (Morey, 2008); ***$p < 0.001$.

Next, we tested for spatial specificity of the illusory shape-related response by contrasting illusory shape responses for the left triangle with illusory shape responses for the right triangle during the easy task. This time, we found positive clusters in the contralateral (right) hemisphere only, in the EVC (V1–V3), hV4, V3a, V3b, and LO1. Whole-brain group results with significant clusters for the spatially specific illusory shape responses are shown in Figure 6*B*.

Finally, we tested for attention modulation of the illusory shape response by contrasting all illusory shape responses in the easy task with illusory shape responses in the hard task. There were no surviving clusters for this analysis. All significant clusters from the illusory shape and spatial specificity analyses are shown in Table 2. Additionally, surface area overlaps of the significant clusters and the areas of the probabilistic visual atlas for illusory shape and spatially specific responses can be found in Table 3.

Control analyses

Since the target frequency was the same in the easy and the hard task, but the hit rate was higher in the former, we tested whether our fMRI results can be explained by the overall differences in motor activity. We compared the average hit frequency, the average miss frequency and the average false alarm frequency per block, considering each stimulus configuration separately. We observed a significant main effect of task in a 2×4 ART ANOVA on the mean frequency of hits ($F_{(1,232)} = 106.707$, $p < 0.001$, $\eta_p^2 = 0.315$), mean frequency of misses ($F_{(1,232)} = 163.105$, $p < 0.001$, $\eta_p^2 = 0.413$) and mean frequencies of false presses $F_{(1,232)} = 47.449$, $p < 0.001$, $\eta_p^2 = 0.17$). Crucially, there was no main effect of the stimulus configuration or interaction in either of the analyses (all p-values ≥ 0.434). This result shows that the participants had on average more hits in the easy task and more misses and false presses in the hard task, but these responses were not influenced by the stimulus configuration. Since in our analysis we always subtract the no illusion condition from each illusory figure condition within the same task, the motor response differences across task should cancel out. It is therefore unlikely that differences in motor responses can explain our observed fMRI effects.

To rule out the effect of motor response on our fMRI results more directly, we performed a control analysis modeling hits, misses, and false alarms in the GLM as nuisance regressors. The results of this analysis showed that there are no substantial differences in the pattern of responses from our main analyses (data not shown). The only p-value that changed from significant to nonsignificant was the response of IPS5 in the ipsilateral triangle condition (changing from 0.034 to 0.053). We therefore conclude that the possible confounding effects of these events on the results were small to insignificant.

Finally, we also tested whether our stimulus, which contained a continuous flicker, engaged other classical dorsal stream regions such as hMT and MST. This analysis showed that neither hMT ($t_{(29)} = -0.271$, $p = 0.788$, $d = -0.05$) nor MST ($t_{(29)} = 0.987$, $p = 0.332$, $d = 0.180$) responded to the illusory diamond. Likewise, there was no contralateral triangle representation in these areas [hMT ($t_{(29)} = -1.365$, $p = 0.081$, $d = -2.492$; MST ($t_{(29)} = 0.075$, $p = 0.94$, $d = 0.014$)]. Overall, the illusory shape responses in the IPS in our study cannot be explained by an unspecific engagement of the dorsal stream as a whole.

Discussion

The results of our study show that IPS areas respond to illusory shapes even when they are not defined by motion. They also indicate that different parietal areas respond to illusory shapes in a different manner. The posterior areas show a spatially specific and attention modulation-independent response. On the other hand, the anterior areas show an attention-dependent response, which is not specific to illusory shape location. Our results thus also show a dissociation between the location-specific and attention-dependent activation during illusory shape perception along the posterior-anterior gradient within the IPS.

Stationary illusory shape responses in the parietal cortex

Several previous fMRI studies already reported illusory shape responses within the superior parietal cortex and the IPS, but those studies relied on motion-defined bistable stimuli which either did or did not produce an impression of a moving illusory shape (Zaretskaya et al., 2013; Grassi et al., 2016, 2018). A bistable paradigm has the advantage of fully matching the illusory and nonillusory conditions. However, it requires participants to track their own subjective experience of the stimulus, which inevitably couples illusory perception and attention. Because of this coupling, previous studies could test neither the topographic specificity of the shape responses, nor their dependence on attention. In the current study, highly controlled and task-irrelevant Kanizsa stimuli allowed us to overcome these constraints, dissociating the illusory figure from the allocation of attentional resources. We demonstrate that illusory content of the Kanizsa shapes is represented within the posterior maps IPS0–3, even

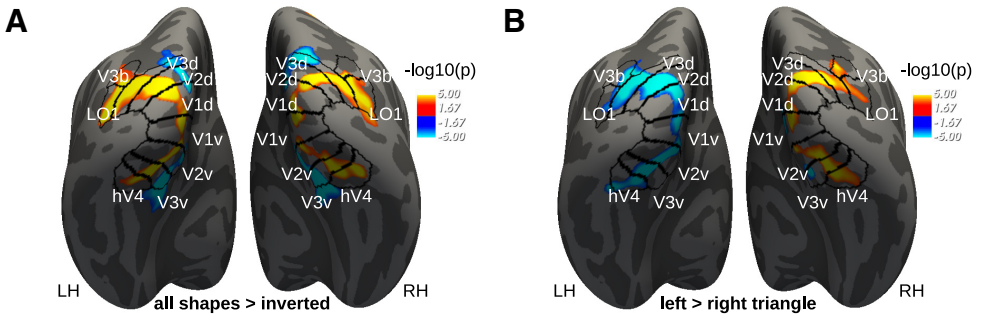

Figure 6. Whole-brain group-level results (corrected for multiple comparisons). ***A***, All illusory shapes > no illusion configuration, easy task. ***B***, Left illusory triangle > right illusory triangle, easy task. Clusters of significant responses are shown on the inflated cortical surface of the fsaverage template. LH, left hemisphere; RH, right hemisphere.

Table 2. Significant clusters of illusory shape and spatially specific responses in the whole brain after correction for multiple comparisons

Gyrus	Size (mm^2)	Max	Vtx max	MNI *X Y Z*	CWP
Shapes > no illusion					
L. lateraloccipital	1588.18	10.165	158,601	−12.7 −101.1 6.6	0.0002
L. lingual	683.32	−9.015	70,275	−20.6 −66.7 −11.3	0.0002
L. cuneus	432.36	−7.640	126,540	−5.4 −93.4 14.7	0.0002
R. pericalcarine	978.75	9.011	34,190	14.3 −89.3 1.3	0.0002
R. lingual	721.15	−11.295	90,642	20.1 −73.6 −6.3	0.0002
R. cuneus	639.84	−7.783	27,606	5.8 −86.3 11.3	0.0002
R. lateraloccipital	452.38	5.841	7091	19.6 −84.8 −10.2	0.0002
R. superiorparietal	96.74	5.328	74,169	21.7 −57.9 56.6	0.02563
LT > RT					
L. lingual	1805.5	−10.336	162,722	−17.6 −84.7 −9.9	0.0002
R. lateraloccipital	890.78	9.781	111,571	10.8 −96.7 13.3	0.0002
R. lateraloccipital	480.96	6.703	70,013	19.7 −84.9 −9.6	0.0002
R. pericalcarine	133.14	−6.109	29,546	16.1 −84.2 4.9	0.00459
R. lingual	108.17	−7.434	53,259	17.1 −76 −8.9	0.01494

LT, left triangle; RT, right triangle; cluster names are represented as hemisphere (L, left; R, right) and gyral-based ROIs (Desikan et al., 2006); max, maximum -log10(p) value; vtx max, index of vertex at the maximum; MNI *X Y Z*, coordinate of the maximum; CWP, cluster-wise *p*-value.

Table 3. Whole-brain results overlap (positive clusters only) with visual topographic areas

	Shapes >no illusion		LT > RT
ROI	LH	RH	RH
V1	20.356	17.670	17.449
V2	24.721	20.016	29.679
V3	38.534	30.098	24.560
hV4	23.697	37.732	38.169
V3a	–	–	2.926
V3b	56.595	13.457	35.805
LO1	71.907	73.353	28.375
LO2	4.598	–	–
IPS3	–	15.606	–
IPS4	–	41.134	–

LT, left triangle; RT, right triangle; LH, left hemisphere; RH, right hemisphere; values represent an overlap between significant clusters and topographic areas expressed as percentage of the respective ROI's surface area. Reported surface area overlaps in V1–V3 represent combined dorsal and ventral part of the respective ROI. Only clusters that overlap with ≥10 vertices with any ROI are shown.

when the shapes are task-irrelevant and attention is engaged elsewhere. This finding implies that parietal topographic areas play a general role in representing illusory content, regardless of the exact perceptual mechanism, be it motion or inducer alignment, that led to its generation.

An outstanding question remains about the exact illusory aspect of the Kanizsa shape driving the parietal activity. Subjective impression induced by a Kanizsa figure includes not only illusory contours, but also illusory surface, which, in turn, is perceived as brighter and closer to the observer (Kogo et al., 2014). In the current study, we focused on illusion-related activity as a whole, without differentiating between single illusory aspects. Future studies are needed to determine the unique contribution of each illusory feature to the IPS activity.

Spatial specificity of shape responses

Our study also revealed that the response of the posterior IPS regions (IPS0–3) is spatially specific. These areas respond stronger to the illusory triangles presented to the contralateral compared with the ipsilateral half of the visual field. Since each IPS map represents the contralateral visual field half, such specificity implies a coarse topographic specificity of illusory shape responses. The topography of the illusory shape responses and its independence from attention in these areas resembles the responses of early visual areas V1 and V2, which show a differentiated pattern of illusory surface enhancement and inducer/background suppression (Kok and de Lange, 2014; Grassi et al., 2017; but see de-Wit et al., 2012). Because of the relatively small surface area and much larger receptive field sizes of the IPS maps compared with V1/V2, it is challenging to show such fine-scale response differences with conventional fMRI. Future studies using high-resolution fMRI at ultrahigh field have the potential to test whether there is a distinction between illusory surface enhancement and inducer suppression (Zaretskaya, 2021).

Dissociation of attention-related and illusion-related response

Another major finding of our study is that the attentional effects were confined to the anterior map IPS4, with a trend in IPS5. These two maps showed a complete absence of responses to peripheral illusory triangles during the more difficult task which forced the allocation of more attentional resources to the fovea. Anterior IPS responses may thus reflect engagement of attentional resources regardless of what engages them. During the easy task illusory shapes may attract attention (Rauschenberger and Yantis, 2001; Senkowski et al., 2005; Kimchi et al., 2016), which leads to higher IPS4 activity for the illusory shape configuration. During the hard task, attention is engaged by a demanding task in the fovea, which leads to equal IPS4 activity for illusory and nonillusory surrounding configuration. The unspecific signaling of attentional engagement could also explain the lack of response lateralization in these areas.

The relationship between attention and grouping is a matter of a long-standing debate (Driver and Baylis, 1998; Treisman and Kanwisher, 1998), fueled in part by findings in patients with

parietal extinction. In such patients, a shape-forming inducer configuration that spans both hemifields facilitates the identification of the inducer in the unattended hemifield, releasing it from extinction (Mattingley et al., 1997; Gögler et al., 2016; Conci et al., 2018; Nowack et al., 2021). In this context, parietal cortex is viewed as an area that accomplishes attentional selection by marking and grouping coherent inducers, which are thought to be represented at the lower levels of the visual hierarchy (Nowack et al., 2021). Our study shows that the posterior maps of the IPS themselves contain a representation of illusory shapes, even if they are task-irrelevant and even under high attentional load. In the context of patient findings this may mean that Kanizsa shape integration happens automatically and preattentively, with the corresponding neural representation propagating up to the levels of the posterior IPS areas, but that the conscious access to and the ability to report on these representations, as it is required in patient studies, is ultimately enabled by attention.

Contrary to the illusory triangles, we found no attentional modulation for the illusory diamond. One potential explanation is that in the case of illusory diamond the locus of attention and the location of the illusory figure coincide. Attentional resources dedicated to the central task could thus also be used to process the foveal illusory diamond surface (Bakar et al., 2008). On the other hand, a contour of the illusory triangle does pass through the central detection task. It could thus be argued that the locus of attention coincides with the illusory surface for triangles as well. An alternative explanation for differences in attentional modulation between diamond and triangles could be the difference in size or saliency of the two shapes. Further studies are needed to tackle the reason for this difference in fMRI effects.

Illusory shape response and predictive coding

Illusory shape responses in the EVC are frequently interpreted in the context of the predictive coding theory (Rao and Ballard, 1999; Kok and de Lange, 2015; Friston, 2018). According to this theory, the response in the topographic representation of the illusory surface increases because the feedback signal contains predictions that do not match with the bottom-up sensory input, resulting in a prediction error. At the same time, the response in the topographic representation of the inducers decreases because there is a match between the prediction and the sensory input (Kok and de Lange, 2014; Grassi et al., 2017). Our findings of the illusory shape-related responses far beyond the EVC are consistent with the hierarchical nature of predictive inference engaging multiple levels of the visual hierarchy (Muckli and Petro, 2013; Kok and de Lange, 2015). The IPS could be enhancing the illusory surface representation on a coarser level and sending back shape information to early visual areas, which are capable of finer and more detailed representation of the subjective content (Roelfsema and de Lange, 2016).

Although the top-down feedback signals are assumed to explain the EVC response profile, it is not known in which areas such feedback signals could originate. One candidate region for the feedback source is the LOC (Chen et al., 2021), which is well known to respond to real (Kourtzi and Kanwisher, 2001) and illusory shapes (Fang et al., 2008; Chen et al., 2020). Our whole-brain results confirm the presence of illusory shape response in both early visual areas and the LOC (LO1). Importantly, our results point to a potential third player in this context, the IPS. Previous bistable perception studies hypothesized that the IPS could be an alternative candidate for sending the feedback signal to V1, especially because it was active even for stimuli that did not evoke the LOC response (Grassi et al., 2018). Interestingly, studies of bistable perception also found a dissociation within the PPC, with the more anterior areas presumably carrying the prediction signals (Kanai et al., 2011; Zaretskaya et al., 2013), and the more posterior areas conveying the prediction error (Kanai et al., 2011). Our results do not support the notion that anterior IPS maps provide the source for the prediction signal, because they showed no illusory shape response during the hard task, while the posterior IPS and the EVC did. Nevertheless, they highlight the functional dissociation within the IPS along the posterior-anterior gradient, which is worth further investigation.

In conclusion, our study shows that the topographic areas along the IPS represent illusory content, with responses in the posterior IPS being spatially specific and the responses in the anterior IPS depending on attentional resources. It remains to be seen whether and how responses within the IPS interact with the well-documented shape responses found in the ventral and early visual areas.

References

Anken J, Tivadar RI, Knebel JF, Murray MM (2018) Brain mechanisms for perceiving illusory lines in humans. Neuroimage 181:182–189.

Bakar AA, Liu L, Conci M, Elliott MA, Ioannides AA (2008) Visual field and task influence illusory figure responses. Hum Brain Mapp 29:1313–1326.

Benson NC, Winawer J (2018) Bayesian analysis of retinotopic maps. Elife 7: e40224.

Brainard DH (1997) The psychophysics toolbox. Spatial Vis 10:433–436.

Brooks JL (2012) Counterbalancing for serial order carryover effects in experimental condition orders. Psychol Methods 17:600–614.

Chen S, Nie QY, Müller HJ, Conci M (2019) Kanizsa-figure object completion gates selection in the attentional blink. Q J Exp Psychol (Hove) 72:1741–1755.

Chen S, Weidner R, Zeng H, Fink GR, Müller HJ, Conci M (2020) Tracking the completion of parts into whole objects: retinotopic activation in response to illusory figures in the lateral occipital complex. Neuroimage 207:116426.

Chen S, Weidner R, Zeng H, Fink GR, Müller HJ, Conci M (2021) Feedback from lateral occipital cortex to V1/V2 triggers object completion: evidence from functional magnetic resonance imaging and dynamic causal modeling. Hum Brain Mapp 42:5581–5594.

Conci M, Groß J, Keller I, Müller HJ, Finke K (2018) Attention as the 'glue' for object integration in parietal extinction. Cortex 101:60–72.

Cox RW (1996) AFNI: software for analysis and visualization of functional magnetic resonance neuroimages. Comput Biomed Res 29:162–173.

Dale AM, Fischl B, Sereno MI (1999) Cortical surface-based analysis. Neuroimage 9:179–194.

Desikan RS, Ségonne F, Fischl B, Quinn BT, Dickerson BC, Blacker D, Buckner RL, Dale AM, Maguire RP, Hyman BT, Albert MS, Killiany RJ (2006) An automated labeling system for subdividing the human cerebral cortex on MRI scans into gyral based regions of interest. Neuroimage 31:968–980.

DeSimone K, Viviano JD, Schneider KA (2015) Population receptive field estimation reveals new retinotopic maps in human subcortex. J Neurosci 35:9836–9847.

de-Wit LH, Kentridge RW, Milner AD (2009) Shape processing area LO and illusory contours. Perception 38:1260–1263.

de-Wit LH, Kubilius J, Wagemans J, Beeck HD (2012) Bistable Gestalts reduce activity in the whole of V1, not just the retinotopically predicted parts. J Vis 12:12.

Driver J, Baylis GC (1998) Attention and visual object segmentation. In: The attentive brain, pp 299–325. Cambridge: The MIT Press.

Eickhoff SB, Heim S, Zilles K, Amunts K (2006) Testing anatomically specified hypotheses in functional imaging using cytoarchitectonic maps. Neuroimage 32:570–582.

Engel SA, Glover GH, Wandell BA (1997) Retinotopic organization in human visual cortex and the spatial precision of functional MRI. Cereb Cortex 7:181–192.

Esteban O, Birman D, Schaer M, Koyejo OO, Poldrack RA, Gorgolewski KJ (2017) MRIQC: advancing the automatic prediction of image quality in MRI from unseen sites Bernhardt BC, ed. PLoS One 12:e0184661.

Esteban O, Markiewicz CJ, Blair RW, Moodie CA, Isik AI, Erramuzpe A, Kent JD, Goncalves M, DuPre E, Snyder M, Oya H, Ghosh SS, Wright J, Durnez J, Poldrack RA, Gorgolewski KJ (2019) fMRIPrep: a robust preprocessing pipeline for functional MRI. Nat Methods 16:111–116.

Fang F, Kersten D, Murray SO (2008) Perceptual grouping and inverse fMRI activity patterns in human visual cortex. J Vis 8:2.

Faul F, Erdfelder E, Lang AG, Buchner A (2007) G*Power 3: a flexible statistical power analysis program for the social, behavioral, and biomedical sciences. Behav Res Methods 39:175–191.

Freud E, Plaut DC, Behrmann M (2016) 'What' is happening in the dorsal visual pathway. Trends Cogn Sci 20:773–784.

Friston K (2018) Does predictive coding have a future? Nat Neurosci 21:1019–1021.

Goebel R, Khorram-Sefat D, Muckli L, Hacker H, Singer W (1998) The constructive nature of vision: direct evidence from functional magnetic resonance imaging studies of apparent motion and motion imagery. Eur J Neurosci 10:1563–1573.

Gögler N, Finke K, Keller I, Müller HJ, Conci M (2016) Object integration requires attention: visual search for Kanizsa figures in parietal extinction. Neuropsychologia 92:42–50.

Goodale MA, Milner AD (1992) Separate visual pathways for perception and action. Trends Neurosci 15:20–25.

Gorgolewski K, Burns CD, Madison C, Clark D, Halchenko YO, Waskom ML, Ghosh SS (2011) Nipype: a flexible, lightweight and extensible neuroimaging data processing framework in python. Front Neuroinform 5:13.

Grassi PR, Zaretskaya N, Bartels A (2016) Parietal cortex mediates perceptual gestalt grouping independent of stimulus size. Neuroimage 133:367–377.

Grassi PR, Zaretskaya N, Bartels A (2017) Scene segmentation in early visual cortex during suppression of ventral stream regions. Neuroimage 146:71–80.

Grassi PR, Zaretskaya N, Bartels A (2018) A generic mechanism for perceptual organization in the parietal cortex. J Neurosci 38:7158–7169.

Greve DN, Fischl B (2009) Accurate and robust brain image alignment using boundary-based registration. Neuroimage 48:63–72.

Greve DN, Fischl B (2018) False positive rates in surface-based anatomical analysis. Neuroimage 171:6–14.

Gulban OF, Nielson D, Poldrack R, Lee J, Gorgolewski C, Vanessasaurus, S Ghosh (2019) poldracklab/pydeface: v2.0.0. Zenodo. Available at https://zenodo.org/record/3524401#.Y0kPHnZByUk.

Hagler DJ, Saygin AP, Sereno MI (2006) Smoothing and cluster thresholding for cortical surface-based group analysis of fMRI data. Neuroimage 33:1093–1103.

Haxby JV, Grady CL, Horwitz B, Ungerleider LG, Mishkin M, Carson RE, Herscovitch P, Schapiro MB, Rapoport SI (1991) Dissociation of object and spatial visual processing pathways in human extrastriate cortex. Proc Natl Acad Sci U S A 88:1621–1625.

Holm S (1979) A simple sequentially rejective multiple test procedure. Scand J Stat 6:65–70.

Kaas JH (1997) Topographic maps are fundamental to sensory processing. Brain Res Bull 44:107–112.

Kanai R, Carmel D, Bahrami B, Rees G (2011) Structural and functional fractionation of right superior parietal cortex in bistable perception. Curr Biol 21:R106–R107.

Kanizsa G (1976) Subjective contours. Sci Am 234:48–53.

Kay M, Elkin LA, Higgins JJ, Wobbrock JO (2021) mjskay/ARTool: ARTool 0.11.0. Zenodo. Available at https://zenodo.org/record/4721941#.Y0kPZ3ZByUk.

Kimchi R, Yeshurun Y, Spehar B, Pirkner Y (2016) Perceptual organization, visual attention, and objecthood. Vision Res 126:34–51.

Kleiner M, Brainard D, Pelli D (2007) What's new in Psychtoolbox-3? Perception 36:1–16.

Kogo N, Drożdżewska A, Zaenen P, Alp N, Wagemans J (2014) Depth perception of illusory surfaces. Vision Res 96:53–64.

Kok P, de Lange FP (2014) Shape perception simultaneously up- and downregulates neural activity in the primary visual cortex. Curr Biol 24:1531–1535.

Kok P, de Lange FP (2015) Predictive coding in sensory cortex. In: An introduction to model-based cognitive neuroscience (Forstmann BU, Wagenmakers EJ, eds), pp 221–244. New York: Springer New York.

Kok P, Bains LJ, van Mourik T, Norris DG, de Lange FP (2016) Selective activation of the deep layers of the human primary visual cortex by top-down feedback. Curr Biol 26:371–376.

Konen CS, Kastner S (2008) Representation of eye movements and stimulus motion in topographically organized areas of human posterior parietal cortex. J Neurosci 28:8361–8375.

Kourtzi Z, Kanwisher N (2001) Representation of perceived object shape by the human lateral occipital complex. Science 293:1506–1509.

Larsson J, Amunts K, Gulyás B, Malikovic A, Zilles K, Roland PE (1999) Neuronal correlates of real and illusory contour perception: functional anatomy with PET: neuronal correlates of illusory contour perception. Eur J Neurosci 11:4024–4036.

Lee TS, Nguyen M (2001) Dynamics of subjective contour formation in the early visual cortex. Proc Natl Acad Sci U S A 98:1907–1911.

Maertens M, Pollmann S, Hanke M, Mildner T, Möller H (2008) Retinotopic activation in response to subjective contours in primary visual cortex. Front Hum Neurosci 2:2.

MathWorks (2019) MATLAB. Natick: The MathWorks Inc.

Mattingley JB, Davis G, Driver J (1997) Preattentive filling-in of visual surfaces in parietal extinction. Science 275:671–674.

Mendola JD, Dale AM, Fischl B, Liu AK, Tootell RBH (1999) The representation of illusory and real contours in human cortical visual areas revealed by functional magnetic resonance imaging. J Neurosci 19:8560–8572.

Morey RD (2008) Confidence intervals from normalized data: a correction to Cousineau (2005). TQMP 4:61–64.

Muckli L, Petro LS (2013) Network interactions: non-geniculate input to V1. Curr Opin Neurobiol 23:195–201.

Murray MM, Wylie GR, Higgins BA, Javitt DC, Schroeder CE, Foxe JJ (2002) The spatiotemporal dynamics of illusory contour processing: combined high-density electrical mapping, source analysis, and functional magnetic resonance imaging. J Neurosci 22:5055–5073.

Murray MM, Foxe DM, Javitt DC, Foxe JJ (2004) Setting boundaries: brain dynamics of modal and amodal illusory shape completion in humans. J Neurosci 24:6898–6903.

Nowack L, Finke K, Biel AL, Keller I, Müller HJ, Conci M (2021) Attention capture by salient object groupings in the neglected visual field. Cortex 138:228–240.

Pelli DG (1997) The VideoToolbox software for visual psychophysics: transforming numbers into movies. Spat Vis 10:437–442.

Rao RPN, Ballard DH (1999) Predictive coding in the visual cortex: a functional interpretation of some extra-classical receptive-field effects. Nat Neurosci 2:79–87.

Rauschenberger R, Yantis S (2001) Attentional capture by globally defined objects. Percept Psychophys 63:1250–1261.

Roelfsema PR, de Lange FP (2016) Early visual cortex as a multiscale cognitive blackboard. Annu Rev Vis Sci 2:131–151.

RStudio Team (2021) RStudio: integrated development environment for R. Boston: RStudio, PBC.

Schluppeck D, Glimcher P, Heeger DJ (2005) Topographic organization for delayed saccades in human posterior parietal cortex. J Neurophysiol 94:1372–1384.

Schneider KA, Richter MC, Kastner S (2004) Retinotopic organization and functional subdivisions of the human lateral geniculate nucleus: a high-resolution functional magnetic resonance imaging study. J Neurosci 24:8975–8985.

Senkowski D, Röttger S, Grimm S, Foxe JJ, Herrmann CS (2005) Kanizsa subjective figures capture visual spatial attention: evidence from electrophysiological and behavioral data. Neuropsychologia 43:872–886.

Sereno MI, Dale AM, Reppas JB, Kwong KK, Belliveau JW, Brady TJ, Rosen BR, Tootell RBH (1995) Borders of multiple visual areas in humans revealed by functional magnetic resonance imaging. Science 268:889–893.

Sereno MI, Pitzalis S, Martinez A (2001) Mapping of contralateral space in retinotopic coordinates by a parietal cortical area in humans. Science 294:1350–1354.

Silver MA, Kastner S (2009) Topographic maps in human frontal and parietal cortex. Trends Cogn Sci 13:488–495.

Silver MA, Ress D, Heeger DJ (2005) Topographic maps of visual spatial attention in human parietal cortex. J Neurophysiol 94:1358–1371.

Stanley DA, Rubin N (2003) fMRI activation in response to illusory contours and salient regions in the human lateral occipital complex. Neuron 37:323–331.

Steinman BA, Steinman SB, Lehmkuhle S (1997) Research note transient visual attention is dominated by the magnocellular stream. Vision Res 37:17–23.

Swisher JD, Halko MA, Merabet LB, McMains SA, Somers DC (2007) Visual topography of human intraparietal sulcus. J Neurosci 27:5326–5337.

Tootell RB, Reppas JB, Kwong KK, Malach R, Born RT, Brady TJ, Rosen BR, Belliveau JW (1995) Functional analysis of human MT and related visual cortical areas using magnetic resonance imaging. J Neurosci 15:3215–3230.

Treisman AM, Kanwisher NG (1998) Perceiving visually presented objets: recognition, awareness, and modularity. Curr Opin Neurobiol 8:218–226.

von der Heydt R, Peterhans E, Baumgartner G (1984) Illusory contours and cortical neuron responses. Science 224:1260–1262.

Wandell BA, Dumoulin SO, Brewer AA (2007) Visual field maps in human cortex. Neuron 56:366–383.

Wang L, Mruczek REB, Arcaro MJ, Kastner S (2015) Probabilistic maps of visual topography in human cortex. Cereb Cortex 25:3911–3931.

Wobbrock JO, Findlater L, Gergle D, Higgins JJ (2011) The aligned rank transform for nonparametric factorial analyses using only ANOVA procedures. In: Proceedings of the SIGCHI Conference on Human Factors in Computing Systems, pp 143–146, CHI '11. New York: Association for Computing Machinery.

Wokke ME, Vandenbroucke ARE, Scholte HS, Lamme VAF (2013) Confuse your illusion: feedback to early visual cortex contributes to perceptual completion. Psychol Sci 24:63–71.

Woolrich MW, Jbabdi S, Patenaude B, Chappell M, Makni S, Behrens T, Beckmann C, Jenkinson M, Smith SM (2009) Bayesian analysis of neuroimaging data in FSL. Neuroimage 45:S173–S186.

Yantis S, Schwarzbach J, Serences JT, Carlson RL, Steinmetz MA, Pekar JJ, Courtney SM (2002) Transient neural activity in human parietal cortex during spatial attention shifts. Nat Neurosci 5:995–1002.

Zaretskaya N (2021) Zooming-in on higher-level vision: high-resolution fMRI for understanding visual perception and awareness. Prog Neurobiol 207:101998.

Zaretskaya N, Bartels A (2015) Gestalt perception is associated with reduced parietal beta oscillations. Neuroimage 112:61–69.

Zaretskaya N, Anstis S, Bartels A (2013) Parietal cortex mediates conscious perception of illusory gestalt. J Neurosci 33:523–531.

Zhou H, Friedman HS, von der Heydt R (2000) Coding of border ownership in monkey visual cortex. J Neurosci 20:6594–6611.